Journal of Materials Chemistry A

Hydrolysis-Resistant Heterogeneous Photocatalysts for PET-RAFT Polymerization in Aqueous Environments

Journal:	*Journal of Materials Chemistry A*
Manuscript ID	TA-ART-05-2023-002582.R2
Article Type:	Paper
Date Submitted by the Author:	12-Jul-2023
Complete List of Authors:	Bell, Kirsten; The Pennsylvania State University, Chemical Engineering Hunter, Brock; The Pennsylvania State University, Chemical Engineering Alvarez, Marvin; University of Texas at Dallas, Department of Bioengineering Seera, Sai Dileep Kumar; The Pennsylvania State University, Chemical Engineering Guo, Yiwen; The Pennsylvania State University, Chemical Engineering Lin, Yen-Ting; The Pennsylvania State University, Chemical Engineering Kim, Seong; Pennsylvania State University Pester, Christian; Penn State,

ARTICLE

Hydrolysis-Resistant Heterogeneous Photocatalysts for PET-RAFT Polymerization in Aqueous Environments

Kirsten Bell,[a] Brock Hunter, [a] Marvin Alvarez,[b] Sai Dileep Kumar Seera,[a] Yiwen Guo,[a] Yen-Ting Lin,[a] Seong H. Kim,[a,c,d] and Christian W. Pester [a,c,d,*]

Received 00th January 20xx,
Accepted 00th January 20xx

DOI: 10.1039/x0xx00000x

Solid-supported organic photocatalysts for radical polymerization are promising materials towards more sustainable chemical syntheses and may also open the pathway towards novel (super)hydrophilic materials. This contribution reports on the development of a hydrolysis-resistant heterogeneous photocatalysis platform based on photocatalytic polymer brushes tethered to solid glass supports. The obtained materials circumvent limitations of silane hydrolysis in aqueous conditions and provide well-controlled light-mediated radical polymerization. Moreover, significantly improved longevity and recyclability can be accomplished by adding hydrophobic protective layers that mitigate silane hydrolysis by limiting water-diffusion to reactive sites. We interrogate both the influence of this hydrophobic protective layer and the influence of the hydrophilicity of the photoactive polymer brush on photocatalytic efficacy of the described platform.

Introduction

Photocatalysis uses light as a renewable energy source to drive a plethora of organic[1–4] and polymer chemistries[5–9] while permitting ambient temperatures, pressures, and mild conditions.[10] Photochemistry in water is particularly attractive – from wastewater remediation[11–14] to chemical syntheses.[10,15–17]

Ideally, photocatalysts for application in water should be inert and non-toxic, strongly oxidizing/reducing but chemically stable with tunable band gaps, easy to prepare at low cost, and long-term stable against photobleaching.[14,18] However, as Russo et al. described last year, organic transformations and polymerizations in water that are driven by visible light have received little attention to date.[10] This is surprising, considering there is innate synergy between sustainable photoredox catalysis and water as an environmentally benign solvent to create less hazardous operating conditions. Further, the chemoselectivity and functional group orthogonality of photocatalysis can provide unique benefits for purification while minimizing side product formation.[10] As such, the study of photoredox catalysis in water has the potential to accelerate the development of sustainable synthetic processes spanning a broad range from drug manufacturing to materials engineering.

Light-mediated polymerization in water in particular shows significant potential to broaden the scope of accessible materials that can be synthesized under visible light and ambient conditions.[19–24] This includes reversible deactivation radical polymerization (RDRP) to produce well-defined (super-)hydrophilic polyelectrolytes,[25,26] zwitterionic materials,[27,28] or polyampholytes,[29] all of which have been considered intriguing materials for various applications, including anti-fouling,[30] anti-icing,[31] anti-fogging,[32] and many others.[33,34] Moreover, water as a solvent for RDRP can provide exciting new chemical behaviors to drive unconventional reaction pathways and accelerate advancements in photocatalysis.[17,35–37]

While RDRP in aqueous solutions has been studied intensively,[17,38–42] a more limited body of work exists on light-mediated RDRP in aqueous environments.[36,43–48] Often, the catalysts need to be chemically modified,[43,46] or protonated[49] to create water-soluble equivalents to those used in organic solvents. Examples include a water soluble zinc porphyrin photocatalyst (Zn(II) meso-tetra(4-sulfonato-phenyl)porphyrin, $ZnTPPS^{4-}$) for photoinduced electron transfer-reversible addition-fragmentation chain transfer (PET-RAFT) polymerization or protonated diphenyldihydrophenazine-derivatives for light-mediated atom transfer radical polymerization (ATRP).[43,49] Such approaches however may be synthetically challenging, detrimental to the photocatalyst's performance, or its chemical stability. Nonetheless, polymerization in water has been studied for PET-RAFT,[32,43,45,47] ATRP,[37,49,50] or photoiniferter polymerization.[51]

It becomes clear that practical potential exists, but significant challenges remain to leverage the full potential of

[a] Department of Chemical Engineering, The Pennsylvania State University, University Park, PA 16802, USA.
[b] Department of Bioengineering, University of Texas at Dallas, Richardson, TX 75080, USA.
[c] Department of Materials Science and Engineering, The Pennsylvania State University, University Park, PA 16802, USA.
[d] Department of Chemistry, The Pennsylvania State University, University Park, PA 16802, USA.
† Electronic Supplementary Information (ESI) available: See
DOI: 10.1039/x0xx00000x

aqueous photoredox processes.[10] These include high costs of transition metal-based photocatalysts, inadequate water-solubility of popular aromatic photocatalysts, limited long-term stability, and photobleaching. This creates a need for an inexpensive synthetic platform that mitigates solubility issues, compatibilizes the photocatalysts to allow operation in water, and affords facile catalyst recycling to reduce cost and minimize product contamination.

To this end, heterogeneous photocatalysts have been developed as a promising alternative.[52–55] One approach is the immobilization of photocatalysts onto solid supports – made possibly by the innate ability of photocatalysts to retain their activity when immobilized. Glass (SiO_x) – in the form of nanoparticles, glass wool, optical fibers, or micron-scale beads – provides a low cost and scalable support with good transparency over the required optical spectrum for photocatalysis.[56,57] Moreover, the versatility of silane chemistry provides nearly limitless options for surface functionalization.[58] Using this approach, Shanmugam et al. grafted Eosin Y to silica nanoparticles and showed their efficacy as recyclable PET-RAFT polymerization catalysts.[59] Interestingly, the authors also reported an increased resistance towards photobleaching after surface-immobilization. Teixeira et. al. immobilized various photocatalysts onto aminopropyl triethoxysilane-functionalized glass wool to produce reusable catalysts for the photooxidation of dimethylanthracene.[60] Beyond such immobilized monolayers, we recently reported on a photocatalyst polymer brush-functionalized glass bead platform for light-mediated synthesis of small molecules and polymers via PET-RAFT.[61,62]

Despite their promise, functionalized SiO_x-surfaces as heterogeneous catalysts in water bear inherent limitations. First and foremost, the facile hydrolysis of the silane surface-anchor (-Si-O-) in water can cause leaching of photocatalysts (monomers or polymer brushes). This would contaminate the synthetic product and decrease the ability to efficiently recycle the photocatalysts. Indeed, polymer brushes cleaving from surfaces due to silane hydrolysis has previously been studied by Genzer,[63] de Beer,[64] and Klok,[65] all of whom identified noticeably decreased grafting densities over time – even in humid air. Previous studies[66–68] indicate however that a hydrophobic polymer shell can act as a protective barrier to limit diffusion of water molecules to the polymer/glass interface and prevent polymer brush hydrolysis.[66–68] For example, Paripovic et al. demonstrated the success of a thin poly(methyl methacrylate) (PMMA) layer in a hydrophobic/hydrophilic diblock copolymer brush.[68] Poly(2,2,2-trifluoro ethyl methacrylate) (PTFEMA) is known to generate an even more hydrophobic surface.[69]

Motivated by this approach, we outline below the development of a hydrolysis-resistant heterogeneous photocatalyst for PET-RAFT polymerization. We leverage the tunable backbone chemistry of photoactive polymer brushes – an inherent advantage of our previous photocatalysis platform.[61,62] In detail, we use a protective hydrophobic underlayer to protect the surface-anchor of the polymer brushes from hydrolyzing (see **Figure 1**). We interrogate both PMMA and TFEMA as protective layers and study their ability to prevent polymer brush hydrolysis. We further study how modifying the hydrophilicity of the outermost layer (between methyl acrylate (MA) and 2-hydroxy ethyl acrylate (HEA) comonomers) influences the photocatalytic efficacy in aqueous solution. Because hydrolysis is prevented, the photocatalyst substrates exhibit stability over multiple well-controlled polymerization cycles after catalyst recycling through simple filtration.

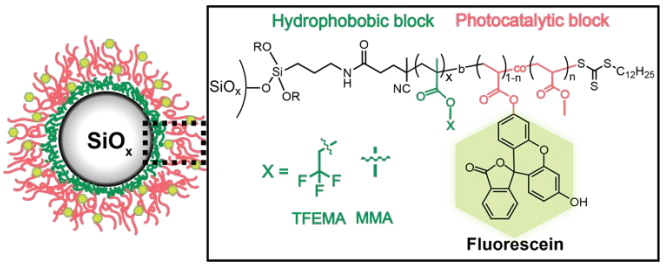

Figure 1. The chemical structure of incorporating a hydrophobic protective shell (PTFEMA or PMMA) diblock copolymer brush for the prevention of hydrolysis. The hydrophobic-*block*-photoactive polymer brush is tethered to a solid SiO_x support (micron-scale bead) and can be used for heterogeneous photocatalysis. The cartoon polymer brush functionalized bead is not drawn to scale.

Results and Discussion

Quantifying hydrolysis of the silane anchoring group

Our lab previously demonstrated the successful use of photocatalytic polymer brush-functionalized glass beads ($PC@SiO_x$) for heterogeneous synthesis of polymers via light-mediated PET-RAFT in dimethyl sulfoxide (DMSO).[61] In detail, fluorescein o-acrylate was copolymerized with methyl acrylate via SI-RAFT to produce surface-anchored poly(fluorescein *o*-acrylate-*co*-methyl acrylate) polymer brushes attached to glass surfaces ($FPB@SiO_x$; **Figure 2a**). However, when attempting PET-RAFT in aqueous solutions for the polymerization of hydrophilic monomers, a noticeable discoloration of the reaction solution was visible to the naked eye. In contrast, this discoloration does not occur in DMSO (**Figure S5a**).

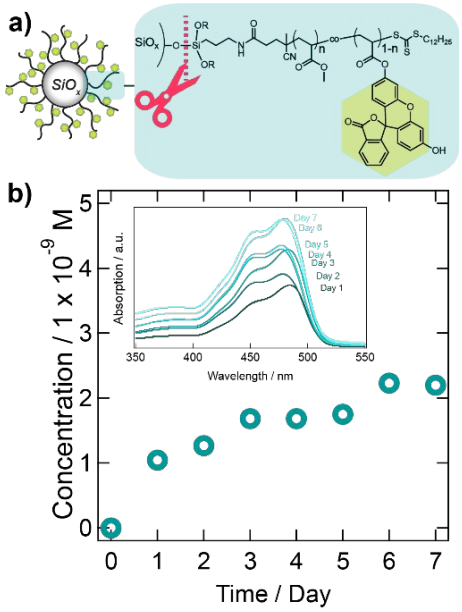

Figure 2. (a) Cartoon schematic of the fluorescein photocatalytic polymer brush glass beads (FPB@SiO_x, not drawn to scale) and the hydrolytic -Si-O- bond highlighted. (b) UV/vis spectroscopy depicts the increasing appearance of fluorescein (photocatalyst) characteristic absorption in water, suggesting hydrolysis and leaching into the solution.

Indeed, as shown in **Figure 2b,** UV/vis spectroscopy showed an increasing intensity of the fluorescein absorption band after stirring the catalyst beads in water for 7 days. ^{1}H-NMR confirmed the presence of the characteristic aromatic fluorescein peaks (δ: 6.55-7.98 ppm in DMSO-d_6, **Figure S5b**). Notably, acrylate-characteristic peaks (δ: 1.76-2.22 ppm in DMSO-d_6, **Figure S5b**) were also detected, suggesting that the entire polymer brush detaches and not merely the photocatalyst motif.

Based on studies outlined above by Genzer,[63] de Beer,[64] and Klok,[65] we hypothesized that hydrolysis of the -Si-O- bonds, connecting the polymer brush to the glass beads is occurring (**Figure 2a**), due to the ingress of water into the brush/glass interface.[70] The de-grafting of the photocatalytic polymer brushes would occur in water, but not in DMSO (as per our observations). However, this hydrolysis also inherently limits the photocatalyst's efficiency and lifetime in aqueous environments while contaminating the synthetic products. To

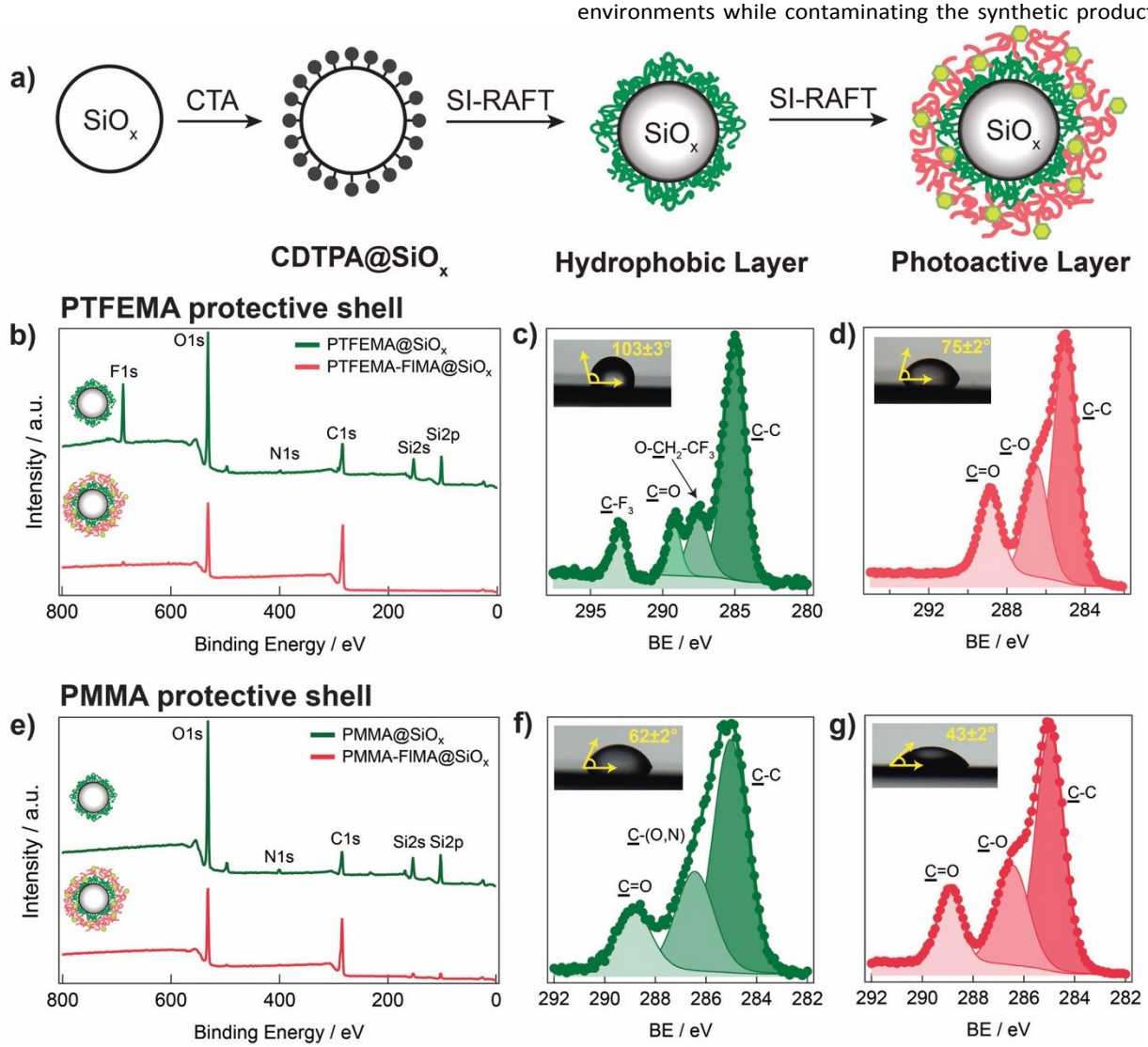

Figure 3. (a) Cartoon schematic of the surface-initiated reversible addition-fragmentation chain transfer polymerization (SI-RAFT) diblock copolymer, not drawn to scale. Surface confirmation of the photoactive diblock copolymer polymer brush substrates (b) (SiO_x)-[F|FIA-MA] and (c) (SiO_x)-[M|FIA-MA] via X-ray photoelectron spectroscopy (XPS). The survey and high-resolution carbon C1s spectra for each layer with measured water contact angle insets.

prevent polymer brush hydrolysis, we were inspired by studies on the addition of a hydrophobic polymer as a protective shell to prevent diffusion of water molecules to the polymer brush/glass interface to enhance the durability of polymer brushes.[66–68]

Synthesis and characterization of hydrophobic-hydrophilic diblock copolymer brush photocatalyst SiO_x beads

An advantage of our previously reported PC-polymer brush platform[61,62] is the ability substitute the comonomers in the surface-initiated RAFT (SI-RAFT) polymerization. This permits the addition of a hydrophobic polymer as a protective shell (**Figure 3a**) to protect the PC-polymer brushes against hydrolysis and extend catalyst stability.

To investigate this approach, the RAFT chain transfer agent (CTA) 4-cyano-4-[(dodecylsulfanylthiocarbonyl)-sulfanyl]pentanoic acid (CDTPA) was anchored to the surface of soda lime silica (SiO_x) glass beads (D_z = 76.3 μm).[61,62] From these CDTPA@SiO_x beads, SI-RAFT of two monomers of varying hydrophobicity, i.e., MMA or TFEMA, was performed. The resulting hydrophobic PMMA or PTFEMA polymer brushes were chain extended by copolymerizing fluorescein *o*-acrylate (FlA, 10 mol.%) with methyl acrylate (MA, 90 mol.%) to produce the final diblock copolymer brush catalysts (**Figure 3a**).

X-ray photoelectron spectroscopy (XPS, **Figure 3**) was used to characterize the obtained poly[MMA-*b*-(FlA-*co*-MA)]@SiO_x (**(SiO_x)-[M|FlA-MA]**) and poly[TFEMA-*b*-(FlA-*co*-MA)]@SiO_x (**(SiO_x)-[F|FlA-MA]**) glass beads. For PTFEMA@SiO_x a characteristic fluorine F1s peak at BE = 688 eV was apparent (**Figure 3b**) and the high resolution C1s spectrum showed the characteristic PTFEMA fingerprint (**Figure 3c**): C-C (285.0 eV), C-O (287.5 eV), C=O (289.0 eV), and C-F (293.0 eV) at atom% ratios of C-C:C-O:C=O:C-F = 7.3:1.7:1:1. A deviation from theoretical expectations (4:1:1:1), i.e., an increased C-C count, is likely due to the 12-carbon CTA chain end. For PMMA@SiO_x, photoelectron spectra showed the expected C1s and O1s peaks (from MMA), an N1s peak (from the amide surface-tether), and Si2s/Si2p peaks from the underlying substrate (**Figure 3e**). High-resolution carbon C1s curve fits were used to identify the individual PMMA carbon environments: C-C (285.0 eV), C-O (286.4 eV), C=O (288.0 eV) were detected at a ratio of C-C:C-O:C=O = 3.9:1.8:1 atom% - again showed an increased C-C count from the CTA (expected: 3:1:1; see **Figure 3f**). Successful copolymerization (chain extension) with FlA and MA was apparent through loss of Si2s/Si2p peaks in the survey spectrum (**Figure 3b,e**). This is a result of a thicker polymer brush exceeding the photoelectron escape depth of approx. 10 nm (see below). For **(SiO_x)-[F|FlA-MA]** the loss of the F1s peak (688 eV) was another indicator for successful polymer brush chain extension (**Figure 3b**). As expected, the final C1s photoelectron spectra for both **(SiO_x)-[F|FlA-MA]** and **(SiO_x)-[M|FlA-MA]** were dominated by the poly(FlMA-co-MA) polymer block (see **Figure 3d** and **Figure 3g**).

Table 1. Summary of the diblock copolymer brush thickness and their respective water contact angle (WCA).

Layer	Thickness[d] (*d*, nm)	Water Contact Angle[e] (*θ*, °)
Unprotected P(FlA-*co*-MA)[a]	12 ± 1	46 ± 1
PTFEMA[b]	16 ± 3	103 ± 3
PTFEMA-*b*-P(FlA-*co*-MA)[c]	34 ± 3	75 ± 2
PTFEMA-*b*-P(FlA-*co*-HEA)[c]	33 ± 3	51 ± 2
PMMA[b]	23 ± 2	62 ± 2
PMMA-*b*-P(FlA-*co*-MA)[c]	38 ± 2	43 ± 2

[a]Reaction conditions of the polymerization were of the following molar ratios of [MA]:[FlA]:[CDTPA]:[AIBN] = [500]:[50]:[1]:[0.25] for 24 hours 75°C under inert conditions. MA = methyl acrylate and FlA = fluorescein *o* -acrylate. [b]Reaction conditions of the hydrophobic monomer were of the following molar ratios of [Monomer]:[CDTPA]:[AIBN] = [100]:[1]:[0.25] for 6 hours at 75°C under inert conditions. PTFEMA = poly(2,2,2-trifluoroethylmethacrylate), PMMA = poly(methyl methacrylate), CDTPA = 4-cyano-4-[(dodecylsulfanylthiocarbonyl)sulfanyl] pentanoic acid, and AIBN = 2,2'-azobis(isobutryronitrile). [c]Reaction conditions of the chain extension polymerization were of the following molar ratios of [MA]:[FlA]:[CDTPA]:[AIBN] = [500]:[50]:[1]:[0.25] for 24 hours 75°C under inert conditions. [d]Thickness determined through J.A. Woollam RC2-D VASE. [e]WCA measurements determined via an in-house setup.

To estimate thicknesses of the diblock copolymer brushes on the SiO_x glass beads, SI-RAFT was concurrently performed on planar glass substrates (see the Supporting Information). Variable angle spectroscopic ellipsometry (VASE) was used to quantify polymer brush layer thicknesses (*d*) for both PMMA and PTFEMA homopolymer brushes as well as the respective **(SiO_x)-[M|FlA-MA]** and **(SiO_x)-[F|FlA-MA]** block copolymer brush films (see **Table 1**). After 24 hours of SI-RAFT reaction time, average film thicknesses of $d_{PTFEMA} \approx 16 \pm 3$ and $d_{PMMA} \approx 23 \pm 2$ nm were obtained for the PTFEMA and PMMA homopolymer brushes, respectively. These findings agree with previous work describing faster polymerization rates for MMA (vs. TFEMA).[71,72] The chain extension of PTFEMA and PMMA polymer brushes resulted in a film thickness increase to $d_{F|FlA\text{-}MA} \approx 34 \pm 3$ nm and $d_{M|FlA\text{-}MA} \approx 38 \pm 2$ nm, respectively (see **Table 1**).

Water contact angles (θ) were measured to determine the changes in hydrophobicity for the different layers (**Figure 4** insets and **Table 1**). PTFEMA exhibited more hydrophobic properties ($\theta \approx 103 \pm 3°$) than PMMA ($\theta \approx 62 \pm 2°$). An expected increase in hydrophilicity was observed after chain extension with the photoactive fluorescein polymer for both **(SiO_x)-[F|FlA-MA]** ($\theta \approx 75 \pm 2°$) and **(SiO_x)-[M|FlA-MA]** ($\theta \approx 43 \pm 4°$).

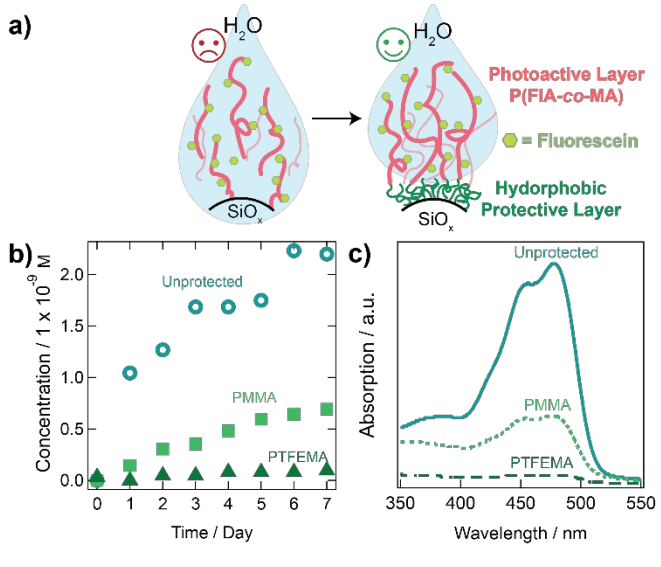

Figure 4. (a) The stability of the fluorescein polymer brush functionalized glass beads (FIMA@SiO_x) in water monitored over a week, comparing the different protective polymer layers (PTFEMA or PMMA) with unprotected FIMA@SiO_x substrates. The polymer brush conformation is not drawn to scale and just for illustration purposes. (b) The UV/vis spectra on day 7, highlighting the characteristic fluorescein absorption at λ_{max} = 480 nm for the determination if hydrolysis occurred.

Mitigating hydrolysis towards heterogeneous photocatalysis in aqueous environments

To examine the effectiveness of the protective hydrophobic blocks, unprotected-, and both PMMA- and PTFEMA-protected polymer brush beads were stirred in water for seven days. UV/vis spectroscopy was used to monitor the concentration changes of hydrolyzed fluorescein-containing polymer brushes with time (see **Figure 4**). As expected, the unprotected **(SiO_x)-[FIA-MA]** shows significant leaching over 7 days up to a concentration above 2 x 10^{-9} M. Both hydrophobic polymer shells significantly improved the stability of the -Si-O- anchoring bond against hydrolysis. **(SiO_x)-[F|FIA-MA]** was observed to be most stable and no significant fluorescein leaching was detected on day 7 (**Figure 4b**). There was however a measurable increase in fluorescein concentration for the PMMA protected coatings – suggesting a hydrophobicity threshold for the protective layers' effectiveness. Due to their improved stability, our focus for studies outlined below was on PTFEMA-reinforced photocatalytic polymer brush films.

Modifying the hydrophilicity of the photoactive layer

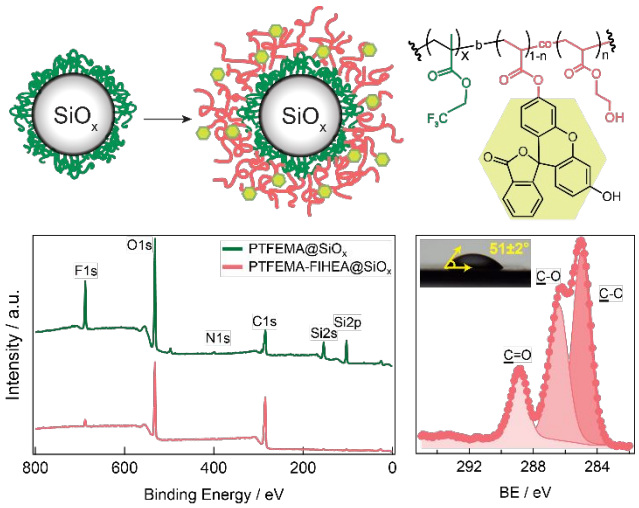

Figure 5. Schematic and XPS survey and high resolution C1s photoelectron spectra for poly[MMA-*b*-(FIA-*co*-MA)]@SiO_x ((SiO_x)-[F|FIA-HEA]) polymer brush-functionalized glass beads. The inset shows a representative water contact angle measurement. The polymer brushes are not drawn to scale as they are on the nanoscale compared to the micron-size surface.

The chain conformation of the photoactive polymer brush layer is anticipated to impact catalytic performance. More catalytic sites are anticipated to be available if the polymer brushes are swollen, i.e., extended into the aqueous environment. To interrogate this, we extended the hydrophobic PTFEMA@SiO_x polymer brush by copolymerizing FIA (10 mol.%) with (i) MA and the (ii) more hydrophilic 2-hydroxyethyl acrylate (HEA; see **Figure 5**). The resulting **(SiO_x)-[F|FIA-MA]** and **(SiO_x)-[F|FIA-HEA]** are anticipated to exhibit different enthalpic interactions with H_2O as described by Flory-Huggins theory.

Synthesis and characterization of **(SiO_x)-[F|FIA-MA]** was outlined above (see **Figure 3a**). Successful formation of **(SiO_x)-[F|FIA-HEA]** copolymer brushes was confirmed via ellipsometry. The initial PTFEMA layer (d_{PTFEMA} = 16 ± 1 nm) increased in thickness increased by $\Delta d \approx 17 \pm 1$ nm for poly(FIA-*co*-HEA) (see **Table 1**). In XPS, block copolymer formation was apparent through the disappearance of the F1s peak (BE = 688 eV) and C-F (293 eV) peak in the C1s spectra (see **Figure 5**). Moreover, a pronounced C-O (286.4 eV) component became apparent – signifying the presence of hydroxyl groups characteristic to the HEA comonomer. Water contact angles on equivalent planar substrates confirmed increased hydrophilicity of **(SiO_x)-[F|FIA-HEA]** ($\theta \approx 51 \pm 2°$) when compared to the initial PTFEMA polymer brushes ($\theta \approx 103 \pm 3°$) and the more hydrophobic **(SiO_x)-[F|FIA-MA]** polymer brushes ($\theta \approx 75 \pm 2°$).

Catalytic Efficacy in Aqueous PET-RAFT polymerization

Aqueous PET-RAFT was conducted to study catalytic efficacy of the developed heterogeneous photocatalysts (see **Figure 6a**). Both **(SiO_x)-[F|FlA-MA]** and **(SiO_x)-[F|FlA-HEA]** were able to polymerize poly(ethylene glycol)methyl ether methacrylate (PEGMEMA, M_n = 300 g mol^{-1}) via PET-RAFT in deionized water (DIW) under blue light irradiation (λ_{max} = 465 nm). The amount of catalyst beads loaded for the aqueous PET-RAFT polymerization was optimized to be about ~1000 mg (**Figure S12**). 4-Cyano-4-(phenylcarbonothioylthio)pentanoic acid (CPADB) and ascorbic acid (AA) were added as CTA and sacrificial electron donor, respectively, at a ratio of [PEGMEMA]:[CPADB]:[AA] = 200:1:2 (see SI). Notably, the CTA chain ends of the fluorescein polymer brush functionalized glass beads were removed prior to these studies to prevent side reactions at the catalyst surface, i.e., incorporation of monomer into the polymer brush backbone.

Figure 6b illustrates that both MA- and HEA-based PTFEMA-protected fluorescein copolymer brush functionalized glass beads successfully accomplished the PET-RAFT of PEGMEMA in water. Experimental molecular weights (as determined via ^{1}H NMR spectroscopy) increased linearly with monomer conversion and were in good agreement with theoretically predicted molecular weights. Molecular weight distributions were measured via gel permeation chromatography (GPC) and remained low ($Đ$ < 1.4) throughout the polymerization (up to 90% monomer conversion), confirming a reversible deactivation radical polymerization mechanism. Control experiments indicated no polymerization in the absence of photocatalyst and without irradiation (**Table S1**), emphasizing the need for the fluorescein polymer brush functionalized glass beads to drive the PET-RAFT polymerization. Without addition of CPADB, free radical polymerization occurred to produce PEGEMEMA with broad molecular weight distribution ($Đ$ = 3.22, **Figure S9a** and **Table S1**). In the absence of ascorbic acid, polymerization occurred slower, achieving 58% conversion of monomer after 12 hours (in comparison to **(SiO_x)-[F|FlA-HEA]** at 73%). We would also like to note that preliminary studies into expanding monomer scope yielded low detectable conversions or high dispersities for non-methacrylic monomers. Further studies in optimizing the present system are necessary, and ongoing in our laboratory, to expand the utility of the present system towards other monomers.

Aqueous PET-RAFT polymerization of PEGMEMA was also conducted in basic and acidic environments to determine the effect of pH (**Figure S11**). In acidic conditions (pH~4), the polymerization rate increases 1.4-fold in comparison to the normal and neutral conditions, whereas under basic conditions (pH~10), the polymerization rate decreases by 50%. For both environments, control over polymerization was maintained with good agreement between experimental and theoretical molecular weights and dispersities $Đ$ < 1.3.

Reusability of protected photoactive polymer brush heterogeneous photocatalysts

The stability of the protected polymer brush photocatalysts were further investigated through the recycling of multiple PET-RAFT polymerizations of PEGMEMA (**Figure 7**).

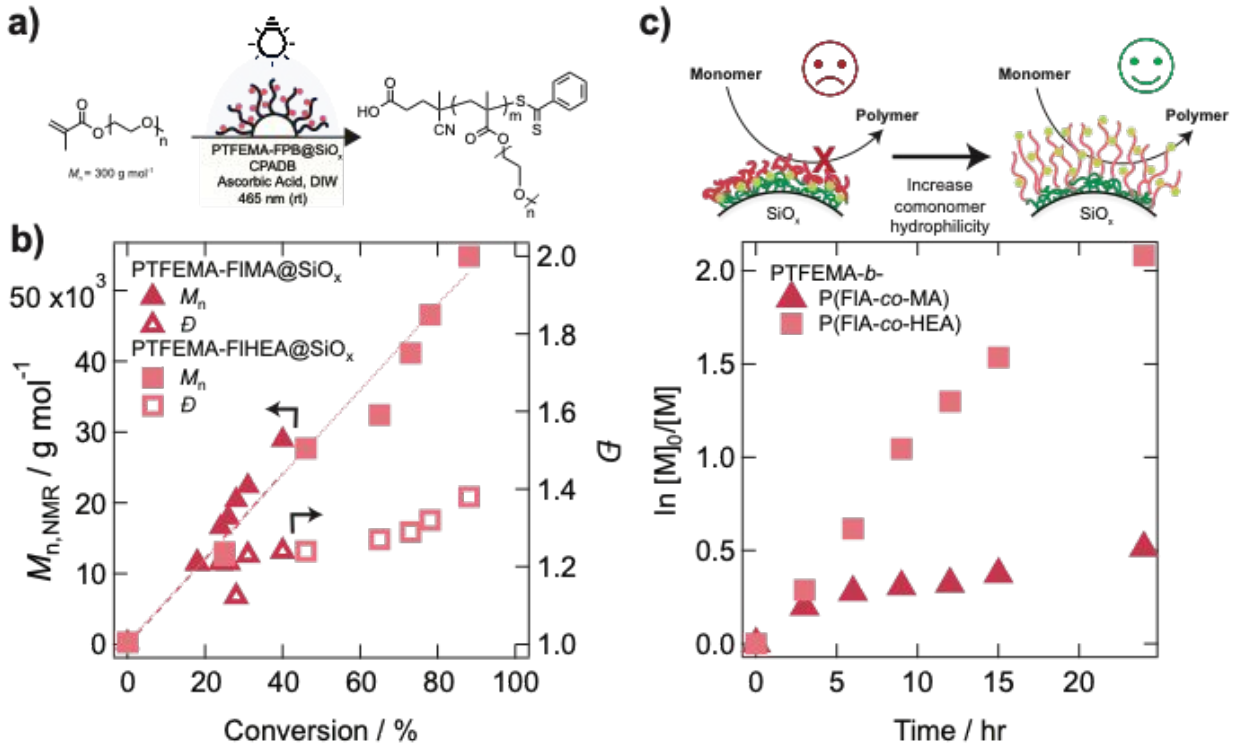

Figure 6. (a) PET-RAFT (chain transfer agent CPADB) of PEGMEMA using photocatalyst polymer brush (FPB)-functionalized SiO_x beads with a protective PTFEMA@SiO_x underlayer polymer block. (b) Number-average molecular weight (as determined by ^{1}H-NMR) and dispersity (obtained via GPC) as a function of PEGMEMA monomer conversion for PET-RAFT using either (SiO_x)-[F|FlA-HEA] (squares) or (SiO_x)-[F|FlA-MA] photocatalysts (triangles). The dashed/dotted lines indicate the theoretical molecular weight for each conversion. (c) Cartoon of how photocatalyst polymer-brush swelling is anticipated to influence monomer access to photocatalytic sites on the SiO_x surface and monomer conversion (for the PET-RAFT polymerizations shown in a) as a function of time, indicating faster PEGMEMA conversion for the more hydrophilic (SiO_x)-[F|FlA-HEA] (vs. (SiO_x)-[F|FlA-MA]). The polymer brushes in the cartoon are not drawn to scale.

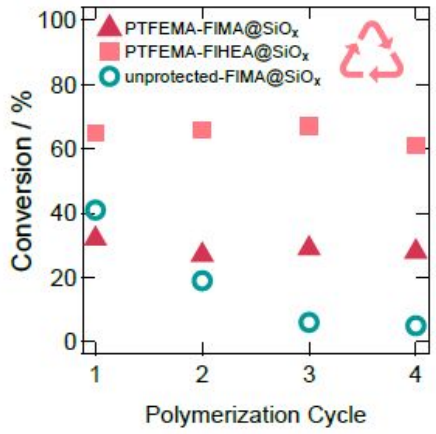

Figure 7. PEGMEMA monomer conversion for 4 consecutive 12 hour PET-RAFT polymerizations using different photocatalysts: (SiO_x)-[F|FIA-HEA] (squares), (SiO_x)-[F|FIA-MA], (triangles), and unprotected (SiO_x)-[FIA-HEA] (spheres).

Both **(SiO_x)-[F|FIA-MA]** and **(SiO_x)-[F|FIA-HEA]** glass beads maintained catalytic activity after four consecutive 12-hour polymerization cycles with an average of 29 ± 2% and 65 ± 3% PEGMEMA conversion, respectively. In comparison, the unprotected **(SiOx)-[FIA-MA]** substrates exhibited a decrease in conversion after just 2 recycles from 41% to 6%. This 85% decrease in conversion confirms the significance of a hydrophobic protective layer to sustain the long-term function of polymer brush-based heterogenous photocatalysts in aqueous environments.

Influence of brush conformation in aqueous environments

As evident from **Figure 6b**, both **(SiO_x)-[F|FIA-MA]** and **(SiO_x)-[F|FIA-HEA]** produced well-defined poly(PEGMEMA) polymers. However, significant differences were observed in polymerization rates (see **Figure 6c**). To explain this, we hypothesized that swelling of the hydrophilic FIA-co-HEA polymer brush in water can increase access of reactants to the photocatalytic sites – thereby increasing reaction rates. In-situ ellipsometry swelling experiments using a 500 μL horizontal liquid cell and vibrational sum frequency generation spectroscopy (SFG) were conducted to test this hypothesis.

The swelling ratio (SR) of photocatalytic polymer brushes was characterized by the ratio between solvated (in H_2O) and dry film thicknesses (d_{wet}/d_{dry}). For **(SiO_x)-[F|FIA-MA]**, the swelling ratio was determined as $SR_{[F|FIA\text{-}MA]}$ = 0.95 and $SR_{[F|FIA\text{-}MA]\text{-}CER}$ = 0.91, where CER is the CTA chain-end removed equivalent of the polymer brush. This indicated no significant penetration of H_2O into the outer FIA-co-MA component of the surface-tethered block copolymer brush. In contrast, the more hydrophilic **(SiO_x)-[F|FIA-HEA]** coatings showed more significant polymer brush swelling, i.e., extended polymer brush conformation ($SR_{[F|FIA\text{-}HEA]}$ = 1.36 and $SR_{[F|FIA\text{-}HEA]\text{-}CER}$ = 1.27). This helps explain the differences in polymerization rates as less swollen catalysts limit access of reactants to photocatalysts within the brush. As a result, photocatalysis is confined to the outermost polymer/water interface. In contrast, penetration of hydrophilic monomers and growing chain ends into the **(SiO_x)-[F|FIA-HEA]** polymer brushes are anticipated to provide increased rates of polymerizations – as we indeed observed (**Figure 6b**).

SFG further corroborated our hypothesis and spectra were recorded for four different polymer brushes on flat glass substrates: **(SiO_x)-[F|FIA-MA]**, **(SiO_x)-[F|FIA-MA]-CER**, **(SiO_x)-[F|FIA-HEA],** and **(SiO_x)-[F|FIA-HEA]-CER**. The **(SiO_x)-[F|FIA-MA]** and **(SiO_x)-[F|FIA-HEA]** brushes and the same brushes with the CTA chain-end removed (CER) were produced on flat glass substrates and their conformational changes upon exposure to dry air and liquid water were probed with SFG. Due to the noncentrosymmetry requirement of the nonlinear optical effect, SFG is sensitive to the non-centrosymmetric arrangement of functional groups at the substrate/brush interface and the brush/environment interface.[73] **Figure 8** compares the SFG spectra of the four polymer brushes collected in dry air and liquid water environments. Since the hydrophobic PTEMA block effectively prevents the ingress of water to the silane anchor (-Si-O-) site (**Figure 4b**), we can rule out any structural change in the substrate/brush region, and the difference between the air and water spectra can be interpreted in terms of conformational changes in the top region of the brush.

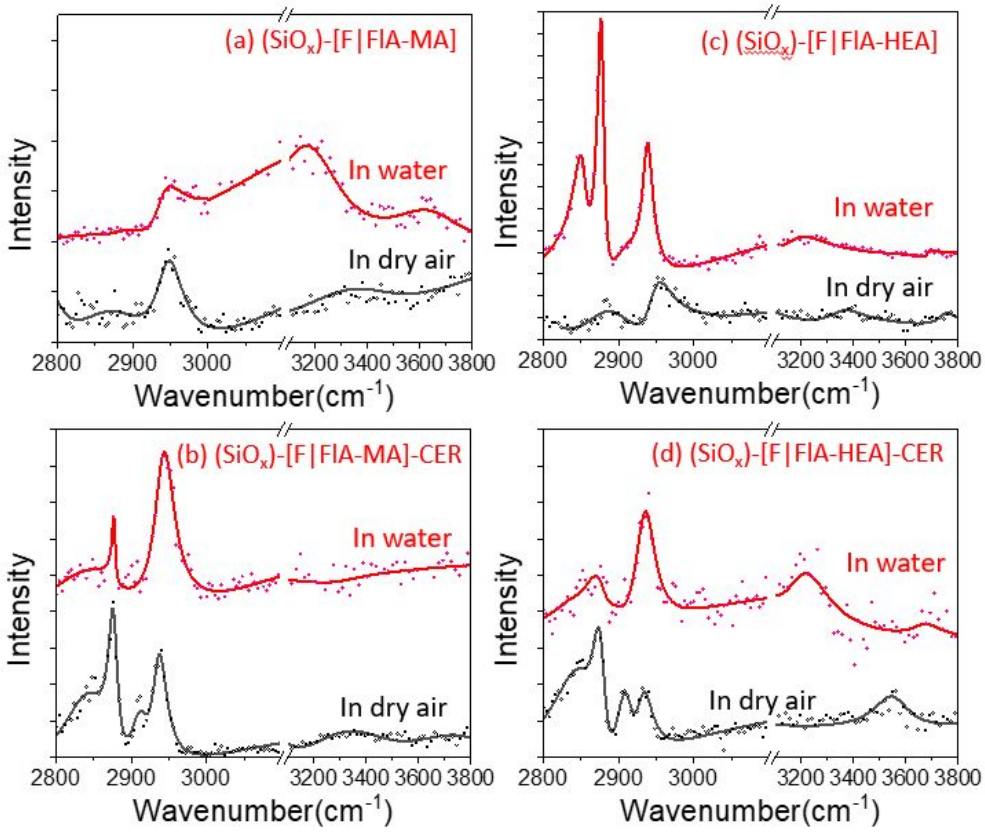

Figure 8. SFG spectra of (a) (SiO_x)-[F|FIA-MA], (b) (SiO_x)-[F|FIA-MA]-CER, (c) (SiO_x)-[F|FIA-HEA], and (d) (SiO_x)-[F|FIA-HEA]-CER brushes on flat substrates in dry air and in liquid water. The polarization combination was s- for SFG signal, s-for 532nm input beam, and p-for tunable IR beam.

In the dry air spectrum in **Figure 8a**, the alkyl stretch signal in the 2800-3000 cm^{-1} region is very weak and the OH stretch signal negligible. This indicates the surface of the **(SiO_x)-[F|FIA-MA]** polymer brush is highly disordered. When it is immerses in water, the OH stretch signal shows a relatively strong and broad peak centered at ~3200 cm^{-1}. This can be attributed to the formation of the "ice-like" water structure at the interface with the hydrophobic **(SiO_x)-[F|FIA-MA]** brush (water contact angle = 75 ±2°; **Figure 3d**). A similar phenomenon was reported for the interface of water and the $C_{16}H_{33}$ self-assembled monolayer (SAM).[74] When the -SC(=S)S-$C_{12}H_{25}$ chain end is removed (**Figure 8b**), the **(SiO_x)-[F|FIA-MA]-CER** brush shows the symmetric stretch of CH_3 group at 2870 cm^{-1}, which implies that the brush surface is mostly populated by the MA group. The aromatic C-H signal is negligible in the SFG spectrum; this might be due to the poor ordering of bulky FIA group at the surface. Upon immersion of **(SiO_x)-[F|FIA-MA]-CER** into water, the ice-like water peak is not observed in the SFG spectrum. This implies that water molecules are not highly order at the interface, probably due to the reduction of the hydrophobicity and the presence of polar MA groups at the surface.

Like the **(SiO_x)-[F|FIA-MA]** brush, the **(SiO_x)-[F|FIA-HEA]** brush surface looks quite disordered in air (**Figure 8c**). However, upon immersion of **(SiO_x)-[F|FIA-HEA]** into water, the strong SFG signals of the long alkyl chain end group appear, while the ice-like OH signal is relatively weak. This can be interpreted with the fact that the **(SiO_x)-[F|FIA-HEA]** brush swells in water (as suggested by in-situ VASE experiment; SR = 1.36). When water ingresses into the hydrophilic HEA region, the non-centrosymmetry at the brush/water interface is reduced; thus, the SFG signal of H_2O molecules at the interface becomes weak. The strong SFG signal of the alkyl stretch region in **Figure 8c** is similar to the SFG features of the poorly-packed $C_{16}H_{33}$ self-assembled monolayer (SAM).[74] From this, it can be deduced

that the $C_{12}H_{25}$ chain ends are somewhat stretched out into the aqueous phase. This conformation might be induced to allow diffusion of water into the HEA region inside the brush. This also explains the good photocatalytic activity of **(SiO_x)-[F|FlA-HEA]**, i.e., faster PET-RAFT of PEGMEMA in water than **(SiO_x)-[F|FlA-MA]** (**Figure 6c**). When the chain end is removed, the **(SiO_x)-[F|FlA-HEA]-CER** brush does not show this strong and well-resolved alkyl signal in the SFG spectrum collected in water (**Figure 8d**). The **(SiO_x)-[F|FlA-HEA]-CER** brush exhibits a weak SFG peak at ~3550 cm^{-1} in dry air, which could be attributed to weakly hydrogen-bonded OH group of the HEA side chain.

Conclusions

We have improved the lifetime and catalytic efficiency of previously established photocatalytic polymer brush heterogeneous catalysts for aqueous environments. A thin hydrophobic layer of PMMA or PTFEMA was incorporated prior to the fluorescein photoactive polymer brush layer. Both PMMA and TFEMA helped reduce (or prevent) the hydrolysis of the -Si-O- surface anchoring bonds. While PTFEMA enhanced stability in water more than the PMMA coating, both diblock polymer brush systems significantly decreased degrafting compared to unprotected substrates. The protected heterogeneous photocatalysts successfully polymerized PEGMEMA in aqueous media via PET-RAFT polymerization to provide well-defined polymers with narrow molecular weight distributions. Furthermore, polymer brush conformation of the fluorescein-containing polymer block considerably influenced photocatalytic performance. The hydrophobic comonomer methyl acrylate decreased the polymerization rate when compared to a hydrophilic comonomer 2-hydroxyethyl acrylate in the photoactive polymer brush backbone. This suggests that the swelling behavior of the hydrophilic matrix improves accessibility of reactants to the photocatalyst within the polymer brush – as we confirmed by in-situ ellipsometry and sum frequency generation (SFG) spectroscopy. This different swelling behavior in turn impacts the reactivity of the photoactive polymer brush as the collapsed polymer conformation of the hydrophobic polymer brushes prevents the access of monomer to the catalytic sites. Overall, the designed protected photocatalytic polymer brush functionalized glass beads platform has potential to significantly enhance organic photochemistry in water and unify the benefits of mild photoredox and heterogeneous catalysis in environmentally friendly solvents.

Author Contributions

All authors approved the final version of the manuscript. K. Bell worked on experiments, writing, and analysis, B. Hunter synthesized the polymer brush surfaces and performed XPS to confirm surface functionalization. M. Alvarez initiated the experiments of the hydrophobic protective layer for the prevention of hydrolysis. S. D. K. Seera collected ellipsometry data. Y. Guo and Y. Lin performed the SFG measurements on the glass surface and S.H. Kim interpreted the SFG spectra. We appreciate help by Rachel Behrens and the NSF BIOPACIFIC MIP (UC Santa Barbara) for GPC analysis.

Corresponding Author

*pester@psu.edu

Conflicts of interest

There are no conflicts to declare.

Acknowledgements

C.W.P. acknowledges the National Science Foundation for financial support (NSF CBET Award #2143628) M.A. was supported by REU grant NSF EEC-1950639. The authors would like to thank Winters Guo and Prof. Gina Noh for UV/vis DR support. In addition, the authors would like to acknowledge Axalta for supporting the SFG data collection.

References

1 R. A. Angnes, Z. Li, C. R. D. Correia and G. B. Hammond, *Org Biomol Chem*, 2015, **13**, 9152–9167.

2 R. C. McAtee, E. J. McClain and C. R. J. Stephenson, *Trends Chem*, 2019, **1**, 111–125.

3 N. A. Romero and D. A. Nicewicz, *Chem Rev*, 2016, **116**, 10075–10166.

4 M. H. Shaw, J. Twilton and D. W. C. MacMillan, *Journal of Organic Chemistry*, 2016, **81**, 6898–6926.

5 M. Chen, M. Zhong and J. A. Johnson, *Chem Rev*, 2016, **116**, 10167–10211.

6 S. Chatani, C. J. Kloxin and C. N. Bowman, *Polym Chem*, 2014, **5**, 2187–2201.

7 X. Pan, M. A. Tasdelen, J. Laun, T. Junkers, Y. Yagci and K. Matyjaszewski, *Prog Polym Sci*, 2016, **62**, 73–125.

8 N. Corrigan, J. Yeow, P. Judzewitsch, J. Xu and C. Boyer, *Angewandte Chemie International Edition*, 2019, **58**, 5170–5189.

9 Y. Yagci, S. Jockusch and N. J. Turro, *Macromolecules*, 2010, **43**, 6245–6260.

10 C. Russo, F. Brunelli, G. C. Tron and M. Giustiniano, *J Org Chem*, , DOI:10.1021/acs.joc.2c00805.

11 J. J. Rueda-Marquez, I. Levchuk, P. Fernández Ibañez and M. Sillanpää, *J Clean Prod*, 2020, 258, 1–13.

12 S. I. S. Mashuri, M. L. Ibrahim, M. F. Kasim, M. S. Mastuli, U. Rashid, A. H. Abdullah, A. Islam, N. Asikin-Mijan, Y. H. Tan, N. Mansir, N. H. M. Kaus and T. Y. Y. Hin, *Catalysts*, 2020, 10, 1–29.

13 D. B. Miklos, C. Remy, M. Jekel, K. G. Linden, J. E. Drewes and U. Hübner, *Water Res*, 2018, 139, 118–131.

14 R. Marschall, *Eur J Inorg Chem*, 2021, 2021, 2435–2441.

15 S. Barata-Vallejo, D. E. Yerien and A. Postigo, *ACS Sustain Chem Eng*, 2021, 9, 10016–10047.

16 K. Sun, Q. Y. Lv, X. L. Chen, L. B. Qu and B. Yu, *Green Chemistry*, 2021, 23, 232–248.
17 J. Qiu, B. Charleux and K. Matyjaszewski, *Progress in Polymer Science (Oxford)*, 2001, **26**, 2083–2134.
18 G. Ren, H. Han, Y. Wang, S. Liu, J. Zhao, X. Meng and Z. Li, *Nanomaterials*, 2021, 11.
19 J. Heuer, T. Kuckhoff, R. Li, K. Landfester and C. T. J. Ferguson, *ACS Appl Mater Interfaces*, , DOI:10.1021/acsami.2c17607.
20 B. Bayarkhuu, C. Yang, W. Wang, K. A. I. Zhang and J. Byun, *ACS Mater Lett*, 2020, **2**, 557–562.
21 M. Ballestri, E. Caruso, A. Guerrini, C. Ferroni, S. Banfi, M. Gariboldi, E. Monti, G. Sotgiu and G. Varchi, *J Photochem Photobiol B*, 2018, **186**, 169–177.
22 C. Boussiron, M. Le Bechec, L. Petrizza, J. Sabalot, S. Lacombe and M. Save, *Macromol Rapid Commun*, , DOI:10.1002/marc.201800329.
23 T. Kuckhoff, K. Landfester, K. A. I. Zhang and C. T. J. Ferguson, *Chemistry of Materials*, 2021, **33**, 9131–9138.
24 S. Ghasimi, K. Landfester and K. A. I. Zhang, *ChemCatChem*, 2016, **8**, 694–698.
25 M. Kobayashi, M. Terada and A. Takahara, *Faraday Discuss*, 2012, **156**, 403–412.
26 Y. Li, Y. Ko, Y. Lin, D. Kiserow and J. Genzer, *Macromolecules*, 2017, **50**, 8580–8587.
27 Y. Yu, G. J. Vancso and S. de Beer, *Eur Polym J*, 2017, **89**, 221–229.
28 H. Nakano, Y. Noguchi, S. Kakinoki, M. Yamakawa, I. Osaka and Y. Iwasaki, *ACS Appl Bio Mater*, 2020, **3**, 1071–1078.
29 A. Nguyen, E. Dallerba and A. B. Lowe, *Macromol Rapid Commun*, , DOI:10.1002/marc.202200096.
30 C. W. Pester, J. E. Poelma, B. Narupai, S. N. Patel, G. M. Su, T. E. Mates, Y. Luo, C. K. Ober, C. J. Hawker and E. J. Kramer, *J Polym Sci A Polym Chem*, 2016, **54**, 253–262.
31 Y. Guo, J. Bae, Z. Fang, P. Li, F. Zhao and G. Yu, *Chem Rev*, 2020, 120, 7642–7707.
32 M. Fromel, D. M. Sweeder, S. Jang, T. A. Williams, S. H. Kim and C. W. Pester, *ACS Appl Polym Mater*, 2021, **3**, 5291–5301.
33 S. J. Buwalda, T. Vermonden and W. E. Hennink, *Biomacromolecules*, 2017, **18**, 316–330.
34 M. Bahram, N. Mohseni and M. Moghtader, in *Emerging Concepts in Analysis and Applications of Hydrogels*, InTech, 2016.
35 B. de Sterck, R. Vaneerdeweg, F. du Prez, M. Waroquier and V. van Speybroeck, *Macromolecules*, 2010, **43**, 827–836.
36 M. Ouchi, H. Yoda, T. Terashima and M. Sawamoto, *Polym J*, 2012, **44**, 51–58.
37 C. Bian, Y. N. Zhou, J. K. Guo and Z. H. Luo, *Macromolecules*, 2018, **51**, 2367–2376.
38 D. Konkolewicz, P. Krys, J. R. Góis, P. V. Mendonça, M. Zhong, Y. Wang, A. Gennaro, A. A. Isse, M. Fantin and K. Matyjaszewski, *Macromolecules*, 2014, **47**, 560–570.
39 P. V. Mendonca, A. S. R. Oliveira, J. P. M. Ribeiro, A. Castilho, A. C. Serra and J. F. J. Coelho, *Polym Chem*, 2019, **10**, 938–944.
40 M. Fantin, A. A. Isse, K. Matyjaszewski and A. Gennaro, *Macromolecules*, 2017, **50**, 2696–2705.
41 A. B. Lowe and C. L. McCormick, *Progress in Polymer Science (Oxford)*, 2007, 32, 283–351.
42 C. L. McCormick and A. B. Lowe, *Acc Chem Res*, 2004, **37**, 312–325.
43 S. Shanmugam, J. Xu and C. Boyer, *Macromolecules*, 2016, **49**, 9345–9357.
44 R. N. Carmean, T. E. Becker, M. B. Sims and B. S. Sumerlin, *Chem*, 2017, **2**, 93–101.
45 J. Niu, Z. A. Page, N. D. Dolinski, A. Anastasaki, A. T. Hsueh, H. T. Soh and C. J. Hawker, *ACS Macro Lett*, 2017, **6**, 1109–1113.
46 C. Bian, Y. N. Zhou, J. D. Deetz and Z. H. Luo, *Chemical Engineering Journal*, 2019, **362**, 721–730.
47 K. P. McClelland, T. D. Clemons, S. I. Stupp and E. A. Weiss, *ACS Macro Lett*, 2020, **9**, 7–13.
48 P. Bonomi, M. D. Attieh, C. Gonzato and K. Haupt, *Chemistry - A European Journal*, 2016, **22**, 10150–10154.
49 X. Su, P. G. Jessop and M. F. Cunningham, *Macromolecules*, 2019, **52**, 6725–6733.
50 D. A. Corbin and G. M. Miyake, *Chem Rev*, 2022, 122, 1830–1874.
51 R. A. Olson, M. E. Lott, J. B. Garrison, C. L. G. Davidson, L. Trachsel, D. I. Pedro, W. G. Sawyer and B. S. Sumerlin, *Macromolecules*, , DOI:10.1021/acs.macromol.2c01239.
52 L. Zhang, G. Ng, N. Kapoor-Kaushik, X. Shi, N. Corrigan, R. Webster, K. Jung and C. Boyer, *Angewandte Chemie - International Edition*, 2021, **60**, 22664–22671.
53 L. Zhang, X. Shi, Z. Zhang, R. P. Kuchel, R. Namivandi-Zangeneh, N. Corrigan, K. Jung, K. Liang and C. Boyer, *Angewandte Chemie - International Edition*, 2021, **60**, 5489–5496.
54 W. F. Wei, X. Li, K. Jiang, B. Zhang, X. Zhuang and T. Cai, *Angewandte Chemie - International Edition*, , DOI:10.1002/anie.202304608.
55 Y. W. Duan, X. J. Zhang, W. L. Guo, M. Jian, T. Cai and X. Li, *J Mater Chem A Mater*, 2023, **11**, 4639–4650.
56 W. Huang, B. C. Ma, D. Wang, Z. J. Wang, R. Li, L. Wang, K. Landfester and K. A. I. Zhang, *J Mater Chem A Mater*, 2017, **5**, 3792–3797.
57 J. Fan, J. Lu, Z. Sha, W. Zuo, X. Fei and M. Zhu, *Sci China Chem*, 2021, **64**, 1596–1604.
58 X. Qian, K. Fuku, Y. Kuwahara, T. Kamegawa, K. Mori and H. Yamashita, *ChemSusChem*, 2014, 7, 1528–1536.
59 S. Shanmugam, S. Xu, N. N. M. Adnan and C. Boyer, *Macromolecules*, 2018, **51**, 779–790.
60 R. I. Teixeira, N. C. De Lucas, S. J. Garden, A. E. Lanterna and J. C. Scaiano, *Catal Sci Technol*, 2020, **10**, 1273–1280.
61 K. Bell, S. Freeburne, A. Wolford and C. W. Pester, *Polym Chem*, , DOI:10.1039/D2PY00966H.

62 K. Bell, S. Freeburne, M. Fromel, H. J. Oh and C. W. Pester, *Journal of Polymer Science*, 2021, **59**, 2844–2853.

63 Y. Ko and J. Genzer, *Macromolecules*, 2019, **52**, 6192–6200.

64 M. B. Perez, M. Cirelli and S. de Beer, *ACS Appl Polym Mater*, 2020, **2**, 3039–3043.

65 J. Wang and H. Klok, *Angewandte Chemie*, 2019, **131**, 10094–10098.

66 Z. Ding, C. Chen, Y. Yu and S. de Beer, *J Mater Chem B*, 2022, 10, 2430–2443.

67 M. Divandari, E. S. Dehghani, N. D. Spencer, S. N. Ramakrishna and E. M. Benetti, *Polymer (Guildf)*, 2016, **98**, 470–480.

68 D. Paripovic and H. A. Klok, *Macromol Chem Phys*, 2011, **212**, 950–958.

69 H. J. Heo, D. J. Han and E. H. Sohn, *J Fluor Chem*, 2019, **219**, 92–97.

70 D. B. Asay, A. L. Barnette and S. H. Kim, *Journal of Physical Chemistry C*, 2009, **113**, 2128–2133.

71 X. Zhang, C. Zhao, Y. Ma, H. Chen and W. Yang, *Macromol Chem Phys*, 2013, **214**, 2624–2631.

72 A. Rastogi, M. Y. Paik, M. Tanaka and C. K. Ober, in *ACS Nano*, 2010, vol. 4, pp. 771–780.

73 Y. R. Shen, *Fundamentals of Sum-Frequency Spectroscopy*, Cambridge University Press, 2016.

74 J. W. Park, H. Kim and M. Han, *Chem Soc Rev*, 2010, **39**, 2935–2947.